

# Irreversibility and entropy production along paths as a difference of tubular exit rates

Julian Kappler\* and Ronojoy Adhikari

DAMTP, Centre for Mathematical Sciences, University of Cambridge, Wilberforce Road, Cambridge CB3 0WA, UK

(Dated: July 24, 2020)

The appealing theoretical measure of irreversibility in a stochastic process, as the inequality of the probabilities of a trajectory and its time reversal, cannot be accessed directly in experiment due to the vanishing probability of a single trajectory. We regularise this definition by considering, instead, the limiting ratio of probabilities for trajectories to remain in the tubular neighbourhood of a smooth path and its time reversal. We show that this leads to an expression for the pathwise medium entropy production that is in agreement with the formal expression from stochastic thermodynamics and devise a procedure for its measurement as a difference of exit rates from tubes. Applying the procedure to bivariate Langevin dynamics yields excellent agreement between measurement and theory. Our work enables the measurement of irreversibility along individual paths in configuration space.

Stochastic processes without memory have been used to describe the dynamics of physical systems starting with the pioneering work of Rayleigh, Einstein and Smoluchowski [1]. The phenomenological observation that systems out of equilibrium display irreversibility has prompted a search for theoretical measures that enable its quantification. The first of these measures was provided by Kolmogorov [2, 3] by considering the joint distribution of pairs of points along a stochastic trajectory and its time reversal. This characterisation was refined by Ikeda and Watanabe [4] by considering the probabilities for stochastic trajectories to remain in the tubular neighbourhood of a smooth path and its time reversal. This line of thought reached its culmination in the elementary definition of irreversibility as the ratio of probabilities for a trajectory and its reverse in the work of Maes and Netočný [5] and Seifert [6]. This provides the clearest derivation of the plethora of results known as fluctuation theorems [7–13], yields a definition of the medium entropy production as the logarithm of the ratio of the probability of forward and backward paths [6], and has engendered the thriving field of stochastic thermodynamics [13–15].

Despite the theoretical importance of the elementary definition of irreversibility, measurements, in both experiment and simulation, have focussed on ensembles of trajectories [16–19] or systems with discrete state space [20], and the medium entropy production along a single continuous trajectory has not yet been measured directly. This is because the probability of a trajectory (and of its reversal) is, strictly speaking, zero and it is not obvious how to transition from an ensemble of trajectories with finite probability to a single trajectory for which the probability vanishes.

In this Letter, we provide a resolution to this impasse by considering, instead of a single trajectory, the probability of an ensemble to trajectories to remain within the tubular neighbourhood of a smooth path [21, 22]. We define the logarithm of probabilities for forward and backward tubes, as the tube radius goes to zero, as a measure

of irreversibility. We show that this coincides with the stochastic thermodynamic expression for the medium entropy production when the latter is restricted to smooth paths. Since the probability to remain in a finite-radius tube can be measured by the rate of exit of trajectories from the encircling tube [21, 22], we obtain the medium entropy production as a difference of exit rates. Measuring the exit rate requires no knowledge of the underlying process (other than that it is memoryless) and our method, then, yields a model-free route to obtaining the entropy production along individual paths. For two-dimensional Langevin dynamics with a non-equilibrium force, we use this relation to directly infer the medium entropy production along individual paths, and find excellent agreement with the theoretical expectation [6]. Our work thus establishes a protocol for directly measuring irreversibility along individual pathways, and allows us to investigate this phenomenon, experimentally or numerically, in a manner that is more refined than the full ensemble.

*Irreversibility via asymptotic tube probabilities.* For a smooth reference path  $\varphi_t, t \in [0, t_f]$ , we define the sojourn probability that a stochastic trajectory  $\mathbf{x}_t$  remains within a tube of radius  $R$  around  $\varphi$  as  $P_R^\varphi(t) \equiv P(\|\mathbf{x}_s - \varphi_s\| < R \forall s \in [0, t])$ , where  $\|\mathbf{v}\| = (v_1^2 + v_2^2 + \dots + v_N^2)^{1/2}$  denotes the standard Euclidean norm in  $\mathbb{R}^N$ , and where we suppress the dependence on the initial condition of the trajectory inside the tube [21]. Combining the approach to irreversibility via tubes [4] with the single-trajectory medium entropy production [6, 13], we define the medium entropy change along  $\varphi$  in terms of asymptotic tube probabilities as

$$\beta \Delta s_m[\varphi] \equiv \lim_{R \rightarrow 0} \ln \frac{P_R^\varphi(t_f)}{P_R^{\tilde{\varphi}}(t_f)}, \quad (1)$$

with  $\tilde{\varphi}_t \equiv \varphi_{t_f-t}$  the time-reverse of the path  $\varphi$  and where  $\beta^{-1} = k_B T$  denotes the thermal energy with  $k_B$  the Boltzmann constant and  $T$  the absolute temperature. The decay of the sojourn probability  $P_R^\varphi(t)$  is described by  $\alpha_R^\varphi(t)$ , the instantaneous exit rate with which stochas-

tic trajectories leave the tube of radius  $R$  for the first time, as

$$P_R^\varphi(t) = \exp \left[ - \int_0^t \alpha_R^\varphi(s) ds \right], \quad (2)$$

and substituting this into Eq. (1), we obtain

$$\beta \Delta s_m[\varphi] = - \lim_{R \rightarrow 0} \int_0^{t_f} \Delta \alpha_R^\varphi(t) dt, \quad (3)$$

where

$$\Delta \alpha_R^\varphi(t) \equiv \alpha_R^\varphi(t) - \alpha_R^\varphi(t_f - t). \quad (4)$$

Equation (3) relates the medium entropy production along an individual path to observable exit rates, thus enabling to infer the entropy production along an individual trajectory without the need to fit a model. More explicitly, the difference in finite-radius exit rates for forward and backwards path, Eq. (4), can be measured for finite tube radius  $R$  without fitting a model to the data, simply by counting how many sample trajectories leave the tube along forward and backward path [21, 22]. According to Eq. (3), by measuring this exit-rate difference for several finite values of  $R$  and extrapolating the results to  $R \rightarrow 0$ , the medium entropy production  $\Delta s_m$  can be obtained. While Eqs. (1-4) do not assume a model for the stochastic evolution of  $\mathbf{x}_t$ , for a given model the exit rate can be calculated analytically. We now consider the Langevin equation for an  $N$ -dimensional coordinate  $\mathbf{x}_t \equiv (x_1(t), x_2(t), \dots, x_N(t))$ , given in Ito form by

$$d\mathbf{x}_t = \mu \mathbf{F}(\mathbf{x}_t) dt + \sqrt{2\mu k_B T} d\mathbf{W}_t \quad (5)$$

where  $\mu = D/k_B T$  is the mobility with  $D$  the diffusion coefficient,  $\mathbf{F}$  is a deterministic force, and  $d\mathbf{W}_t$  is the Wiener process. While in the present work we only consider forces that do not depend on time explicitly, our approach remains valid for time-dependent forces as long as for time-reversed paths the explicit time-dependence of the force is also reversed [13]. For Langevin dynamics, the leading-order expansion of  $\alpha_R^\varphi(t)$  in the tube radius  $R$  is given by [21]

$$\alpha_R^\varphi(t) = \frac{C_N}{R^2} + \mathcal{L}^\varphi(t) + \mathcal{O}(R^2), \quad (6)$$

where  $C_N$  is a constant which only depends on the dimension  $N$ , and the Onsager-Machlup (OM) Lagrangian  $\mathcal{L}^\varphi$  is given by

$$\mathcal{L}^\varphi = \frac{1}{4D} [\dot{\varphi} - \mu \mathbf{F}(\varphi)]^2 + \frac{1}{2} \text{div}[\mu \mathbf{F}(\varphi)]. \quad (7)$$

Substituting Eq. (7) into the difference of exit rates Eq. (6) for forward- and reverse path, the relation

$$\lim_{R \rightarrow 0} \Delta \alpha_R^\varphi(t) = -\beta \mathbf{F}(\varphi_t) \cdot \dot{\varphi}_t \quad (8)$$

between the limit of exit-rate difference and work rate along  $\varphi$  follows. In turn substituting this into Eq. (1) yields the familiar formula [6, 13]

$$\beta \Delta s_m[\varphi] = \beta \int_0^{t_f} \mathbf{F}(\varphi_t) \cdot \dot{\varphi}_t dt, \quad (9)$$

which relates the medium entropy production and the work performed along  $\varphi$ .

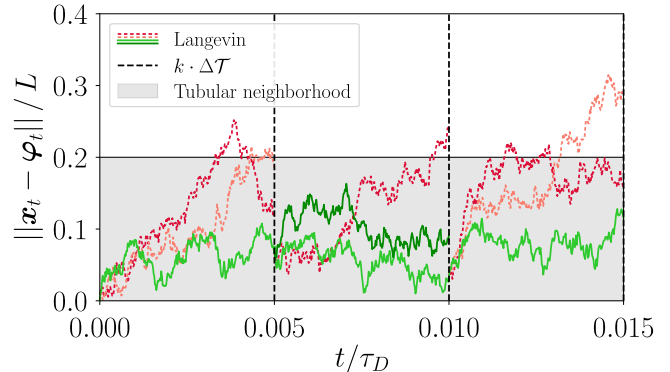


Figure 1. The grey shaded area denotes a tube of radius  $R = 0.2L$  around a reference path  $\varphi$ . We simulate  $M = 3$  Langevin trajectories of duration  $\Delta \mathcal{T} = 0.005 \tau_D$  (vertical dashed lines), all of which start at  $\varphi_0$ . Trajectories which leave the tube (red dotted lines) are discarded, the final positions of the trajectories that stay (green solid lines) are collected. We then again simulate  $M = 3$  Langevin trajectories, each of which starts at a randomly drawn previous final positions. This process is repeated. The small value  $M = 3$  is chosen here for illustration; to calculate exit rates from simulations we use values of the order  $10^5$ , see Appendix A. The reference path  $\varphi \equiv \varphi^{(1)}$  used here is given by Eq. (11) with  $n = 1$ , for the force we use Eq. (10), with  $\theta = 2$ ,  $L\beta F_0 = 5$ .

*Exit rate from cloned trajectories.* To infer the entropy production from finite-radius exit rates, the right-hand side of Eq. (4) needs to be measured for small but finite radius  $R$ . In practice it can be difficult to acquire sufficient data for this measurement, because the number of trajectories which remain inside the tube decreases exponentially with time  $t$ . To measure the exit rate by running a large number of independent simulations starting at  $\varphi_0$ , and counting which fraction remains within the tube until time  $t$ , an unfeasibly large number of simulations would typically be required. To overcome this problem, we employ a cloning algorithm, which is illustrated in Fig. 1; this is a variant of an algorithm recently used to measure relative path probabilities from experimental data [22]. For a given reference path  $\varphi$  and tube radius  $R$ , we simulate  $M$  Langevin trajectories for a short time  $\Delta \mathcal{T}$ , all of which start at  $\varphi_0$ . Trajectories which leave the tube are discarded, the final positions of those trajectories that stay until time  $\Delta \mathcal{T}$  are collected. For times  $t \in [0, \Delta \mathcal{T}]$ , the sojourn probability  $P_R^\varphi(t)$  is then estimated as the fraction of simulated trajectories which

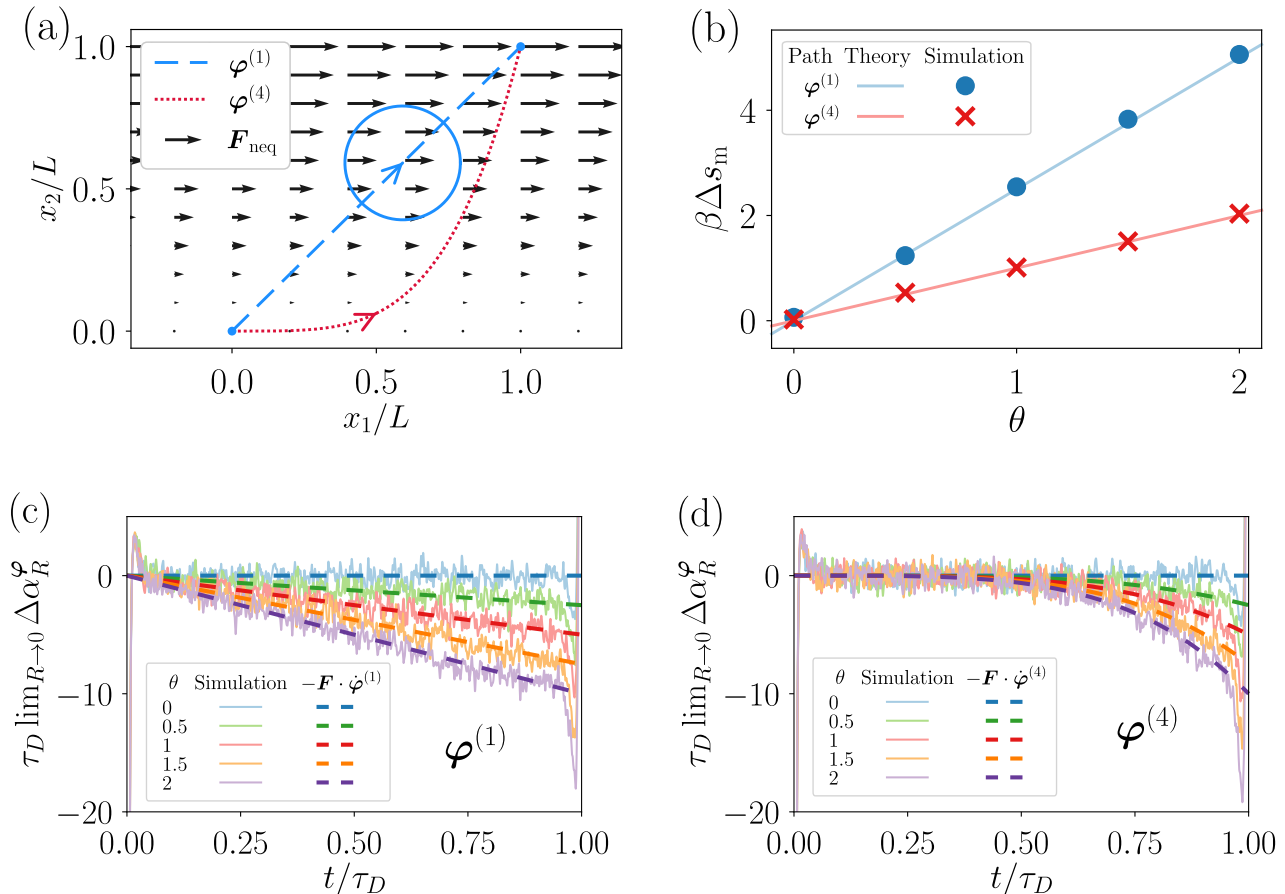


Figure 2. (a) The shear force Eq. (10) is shown as black quiver plot. The path  $\varphi^{(n)}$  defined in Eq. (11) is shown for  $n = 1$  (blue dashed line) and  $n = 4$  (red dotted line), with arrows indicating the forward direction. For  $\varphi^{(1)}$  we include a snapshot of the instantaneous tube of radius  $R/L = 0.2$  around the path (blue circle). (b) The coloured lines denote the theoretical entropy production Eq. (12) as a function of  $\theta$  for  $n = 1$  (blue) and  $n = 4$  (red). The coloured symbols are obtained by evaluating the integral Eq. (3) using the extrapolated measured exit rates shown in subplots (c), (d). (c), (d) The coloured solid lines denote the extrapolation to  $R = 0$  of measured finite-radius exit-rate differences between forward and reverse paths for several values of  $\theta$ . The reference paths are given by Eq. (12) with (c)  $n = 1$  and (d)  $n = 4$ . The coloured dashed line denotes the corresponding theoretical prediction given by the right-hand side of Eq. (8), calculated using the force Eq. (10) with  $L\beta F_0 = 5$ . Numerical data is smoothed using a Hann window of width  $0.005 \tau_D$ .

stay inside the tube until  $t$ . According to Eq. (2), the exit rate is then obtained from the sojourn probability as  $\alpha_R^\varphi(t) = -(\partial_t P_R^\varphi(t))/P_R^\varphi(t)$ . From the final positions of all simulated trajectories that have remained inside the tube until the time  $t = \Delta\mathcal{T}$ , we draw initial positions (using a uniform distribution, and with replacement) for  $M$  new simulated trajectories which are then used to estimate the exit rate for  $t \in [\Delta\mathcal{T}, 2\Delta\mathcal{T}]$ . To obtain the exit rate until a final time  $t_f = K \cdot \Delta\mathcal{T}$ , this process is repeated  $K$  times. For all numerical results shown in this paper, we simulate Eq. (5) using an Euler-Mayurama integrator with timestep  $\Delta t/\tau_D = 10^{-5}$ , where  $\tau_D \equiv L^2/D$  denotes the typical time scale of diffusion over a distance  $L$ . We use  $\Delta\mathcal{T} = 0.005 \tau_D$ , and for the number of trajectories  $M$  we use values of the order of  $10^5$ , which are

chosen dynamically as explained in Appendix A.

*Two-dimensional non-equilibrium example system.* For a length scale  $L$  and a time scale  $\tau$ , we consider the Langevin Eq. (5) for dimension  $N = 2$  with diffusivity  $D = L^2/\tau$ , so that  $\tau_D \equiv L^2/D = \tau$ . We consider a shear force  $\mathbf{F}$  given by

$$\mathbf{F}(\mathbf{x}) = \theta \mathbf{F}_{\text{neq}}(\mathbf{x}) \equiv \frac{\theta F_0}{L} \begin{pmatrix} x_2 \\ 0 \end{pmatrix}, \quad (10)$$

where in the following we fix  $L\beta F_0 = 5$ , so that the dimensionless parameter  $\theta \in \mathbb{R}$  controls the amplitude of the force. The force Eq. (B1) does not admit a potential, and is illustrated as a quiver plot in Fig. 2 (a). We

consider a family of paths

$$\varphi_t^{(n)} = L \left( \frac{t/t_f}{(t/t_f)^n} \right), \quad (11)$$

where  $t \in [0, t_f] \equiv [0, \tau]$  and  $n \in \mathbb{N}$  enumerates the paths. For any  $n$ , the path starts at  $\mathbf{x} = (0, 0)$  and ends at  $\mathbf{x} = (L, L)$ , example paths for  $n = 1$  and  $n = 4$  are shown in Fig. 2 (a). For Eq. (11) and the force Eq. (10), the analytical medium entropy production Eq. (9) is evaluated to

$$\beta \Delta s_m[\varphi^{(n)}] = \frac{L\beta F_0}{n+1} \theta. \quad (12)$$

We now consider Eq. (11) for  $n = 1$ . For  $\theta = 0, 0.5, 1, 1.5, 2$ , we measure the finite-radius exit rate along both  $\varphi^{(1)}$  and its time-reverse  $\tilde{\varphi}^{(1)}$  for radius  $R/L = 0.2, 0.25, 0.3, 0.35, 0.4, 0.45, 0.5$ . We subsequently extrapolate the measured finite-radius exit-rate differences Eq. (4) to vanishing radius by, at each time  $t$ , fitting a quadratic function  $f(t, R) = a(t) + R^2 b(t)$  to the data, and then extrapolating to  $R \rightarrow 0$  as  $\lim_{R \rightarrow 0} \Delta \alpha_R^{\varphi^{(1)}}(t) \equiv a(t)$ . In Fig. 2 (c), the resulting extrapolated exit-rate difference as function of time is compared to the corresponding analytical expectation, given by the right-hand side of Eq. (8), for all values of  $\theta$  considered. We observe that both in the beginning,  $t \lesssim 0.05 \tau_D$ , and at the end of the trajectory,  $t \gtrsim 0.95 \tau_D$ , theory and numerical results deviate; this is because in our cloning algorithm all simulated Langevin trajectories initially start in the center of the tube, so that at the beginning/end we observe the initial relaxation of the initial condition for the forward/reverse path [21]. In Fig. 2 (b) we compare the negative temporal integral over the extrapolated exit rate (blue dots) to the theoretical prediction of the medium entropy production (blue solid line), Eq. (12) with  $n = 1$ . The Langevin results agree perfectly with the theoretical prediction, confirming Eq. (3) and showing that the difference in tubular forward- and reverse exit rates can indeed be used to quantify the entropy production along an individual path without the need of inferring a model. While, contrary to the order in Eq. (3), we first calculate the limit of the exit-rate difference, which we then integrate, any order of these two operations leads to the same results.

To emphasize that our method works for arbitrary paths, we consider a second example path, plotted as red dotted line in Fig. 2 (a) and given by Eq. (11) with  $n = 4$ . We again use the cloning algorithm from Fig. 1 to measure finite-radius exit rates for the same values of  $\theta$  and  $R$  as used for  $\varphi^{(1)}$ . For every value of  $\theta$  we extrapolate the resulting exit-rate differences to  $R = 0$ , and show the result in Fig. 2 (d). As for  $\varphi^{(1)}$ , we find very good agreement between extrapolated exit-rate differences and the analytical limit Eq. 8. We integrate over these curves,

and in Fig. 2 (b) compare the resulting numerically measured entropy production along  $\varphi^{(4)}$  (red crosses) to the theoretical expectation (red solid line), given by Eq. (12) with  $n = 4$ . We find that the simulated entropy production along  $\varphi^{(4)}$  agrees very well with the theoretical expectation.

In Appendix B we furthermore consider another two-dimensional example system, comprised of a circular double-well potential superimposed with a circular nonequilibrium force; the example again confirms the validity and practical applicability of Eq. (3).

*Discussion.* We have shown that the path-wise medium entropy production can be obtained from the exit rate of trajectories from the tube encircling a path, in the limit of the tube radius going to zero. The exit rate can be measured without any knowledge of the underlying dynamics. Our work shows clearly that the most probable paths, which minimise the exit rate, need not be those that maximise their differences and hence provides a method of investigating, in experiment and simulation, the relationship between paths of extremal probability and extremal entropy production [23]. This extends naturally to a comparison of the entropy production along competing pathways between identical initial and final points and allows for a decomposition of the total entropy production into independent components. Our definition of the medium entropy production does not involve non-differentiable stochastic trajectories and thus generalises to processes with configuration-dependent diffusivities in a manner that side-steps delicate issues of stochastic integration (i.e. the Ito-Stratonovic dilemma) [24–26]. The exit rate provides information beyond the entropy production as Eq. 8, with the differential  $\dot{\varphi}_t dt$  chosen along  $N$  linearly independent directions, provides direct information about the drift  $\mathbf{F}$  of the process, without the need to estimate the diffusivity. Our work raises the question of how the medium entropy production could be generalised to tubes of finite radius and what the relationship of such a definition would be to the single-trajectory and full-ensemble measures of entropy production. Finally, our work suggests a generalisation to stochastic field theories with broken detailed balance that are used to describe the fluctuating dynamics of active matter [27].

*Acknowledgements.* Work was funded in part by the European Research Council under the EU's Horizon 2020 Program, Grant No. 740269, and by an Early Career Grant to RA from the Isaac Newton Trust.

## Appendix A: Estimating the number of samples

The algorithm we use to measure exit rates from simulations, illustrated in Fig. 1, relies on repeated simulation of  $M$  independent trajectories. To choose the number  $M$  efficiently for each repetition, we employ the same algorithm as used in Ref. [22]. More explicitly, at the  $k$ -th

repetition ( $k > 1$ ) of the cloning algorithm, we fit a linear function

$$\alpha_{\text{fit}}(t) = a \cdot (t - k \cdot \Delta\mathcal{T}) + b, \quad (\text{A1})$$

to the measured exit rate in the time interval  $[k \cdot \Delta\mathcal{T} - \Delta t_{\text{fit}}, k \cdot \Delta\mathcal{T}]$ , where  $\Delta t_{\text{fit}}/\tau_D = \min\{0.05, \Delta\mathcal{T}/\tau_D\}$ . We then use this fitted exit rate to estimate the expected decay of the sojourn probability for the next iteration duration  $\Delta\mathcal{T}$ , and choose  $M$  such that at the end of the  $k$ -th iteration step we expect to have  $N_{\text{final}}$  trajectories remaining inside the tube. This leads to

$$N_{\text{final}} = M \exp \left[ - \int_{k \cdot \Delta\mathcal{T}}^{(k+1) \cdot \Delta\mathcal{T}} \alpha_{\text{fit}}(s) ds \right], \quad (\text{A2})$$

$$\Leftrightarrow M = N_{\text{final}} \exp \left[ a \frac{\Delta\mathcal{T}^2}{2} + b \Delta\mathcal{T} \right], \quad (\text{A3})$$

and for all exit rates obtained from simulations in the present paper we use  $N_{\text{final}} = 10^5$ .

### Appendix B: Entropy production along closed loops in a circular double well

We here consider a second example system. For a length scale  $L$  and a time scale  $\tau$ , we again consider the overdamped Langevin Eq. (5) for dimension  $N = 2$  with diffusivity  $D = L^2/T$ , so that  $\tau_D \equiv L^2/D = \tau$ . We now consider a force  $\mathbf{F}$

$$\mathbf{F}(\mathbf{x}) = -(\nabla U)(\mathbf{x}) + \theta \mathbf{F}_{\text{neq}}(\mathbf{x}), \quad (\text{B1})$$

which is given as a sum of the gradient of a potential  $U$  and an additional term  $\mathbf{F}_{\text{neq}}$  which is non-conservative, i.e. does not admit a (global) potential. As in the main text, the dimensionless parameter  $\theta \in \mathbb{R}$  controls the amplitude of the non-conservative force, and for  $\theta \neq 0$  this system is a non-equilibrium system. For  $U$  we consider a sombrero potential superimposed with an angular double well, defined as

$$U(\mathbf{x}) = U_0 \cdot \left[ \left( \frac{\|\mathbf{x}\|}{L} \right)^2 - 1 \right]^2 + U_1 \left[ \frac{1 + \cos(2\phi)}{2} \cdot \frac{1 + \exp\left(\frac{1}{10}\right)}{1 + \exp\left(\frac{\|\mathbf{x}\|^2}{10L^2}\right)} - 1 \right], \quad (\text{B2})$$

where  $\|\mathbf{x}\| = \sqrt{x_1^2 + x_2^2}$ ,  $x_1 = \|\mathbf{x}\| \cos(\phi)$ ,  $x_2 = \|\mathbf{x}\| \sin(\phi)$ ; we use  $\beta U_0 = 5$ ,  $\beta U_1 = 2$ . This potential, which is illustrated in Fig. 3 (a), has local minima at  $\mathbf{x} = (L, 0)$ ,  $(-L, 0)$ , and saddle points at  $\mathbf{x} = (0, L)$ ,  $(0, -L)$ . For the non-equilibrium force we consider an angular force

$$\beta \mathbf{F}_{\text{neq}}(\mathbf{x}) = \frac{1}{\|\mathbf{x}\|^2} \begin{pmatrix} -x_2 \\ x_1 \end{pmatrix}, \quad (\text{B3})$$

which illustrated as a quiver plot in Fig. 3 (a).

For the force Eqs. (B1), (B2), (B3), and  $\varphi$  a closed loop, the analytical entropy production Eq. (9) is given by

$$\beta \Delta s_{\text{m}}[\varphi] = 2\pi\Gamma\theta, \quad (\text{B4})$$

where  $\Gamma \in \mathbb{Z}$  is the winding number which quantifies how often the path  $\varphi$  winds counterclockwise around the origin  $\mathbf{x} = \mathbf{0}$ . Thus, for the particular nonequilibrium force Eq. (B3), the theoretical entropy production Eq. (B4) is topological, i.e. only depends on the winding number and not on more details of the path.

We consider two circular paths

$$\varphi_t = L \begin{pmatrix} \cos(2\pi t/t_f) \\ \sin(2\pi t/t_f) \end{pmatrix}, \quad (\text{B5})$$

$$\psi_t = L \begin{pmatrix} \cos(2\pi t^2/t_f^2) \\ \sin(2\pi t^2/t_f^2) \end{pmatrix} + \frac{L}{5} \begin{pmatrix} \sin(10\pi t^2/t_f^2) \\ \sin(2\pi t^2/t_f^2) \end{pmatrix}, \quad (\text{B6})$$

where  $t \in [0, t_f] \equiv [0, \tau]$ . These paths, which both have a winding number  $\Gamma = 1$ , are shown in Fig. 3 (a) as yellow dashed and red dotted lines.

For  $\theta = 0, 0.5, 1, 1.5, 2$  and  $R/L = 0.2, 0.25, 0.3, 0.35, 0.4, 0.45, 0.5$ , we measure the entropy production along the forward- and reverse version of each path  $\varphi$ ,  $\psi$ , using the cloning algorithm illustrated in Fig. 1. We extrapolate the resulting finite-radius exit-rate differences between forward- and reverse path  $R = 0$  as described in the main text, and in Fig. 3 (c), (d) show that the result agrees well with the theoretical prediction Eq. (8) along the paths. Finally, in Fig. 3 (b) we compare the negative temporal integral of the extrapolated exit-rate differences with the expected theoretical entropy production, and find that the numerical and theoretical results agree very well. Thus, also this second example confirms that Eq. (3) can be used to infer the medium entropy production along individual paths directly from exit rates.

\* jk762@cam.ac.uk

- [1] S. Chandrasekhar, "Stochastic Problems in Physics and Astronomy," *Reviews of Modern Physics* **15**, 1–89 (1943).
- [2] A. Kolmogoroff, "Zur Umkehrbarkeit der statistischen Naturgesetze," *Mathematische Annalen* **113**, 766–772 (1937).
- [3] A M Yaglom, "On the statistical reversibility of Brownian motion," *Mat. Sb. (N.S.)* **24 (66)**, 467–492 (1949).
- [4] Nobuyuki Ikeda and Shinzo Watanabe, *Stochastic differential Equations and diffusion processes*, 2nd ed., North-Holland mathematical Library No. 24 (North-Holland [u.a.], Amsterdam, 1989) oCLC: 20080337.

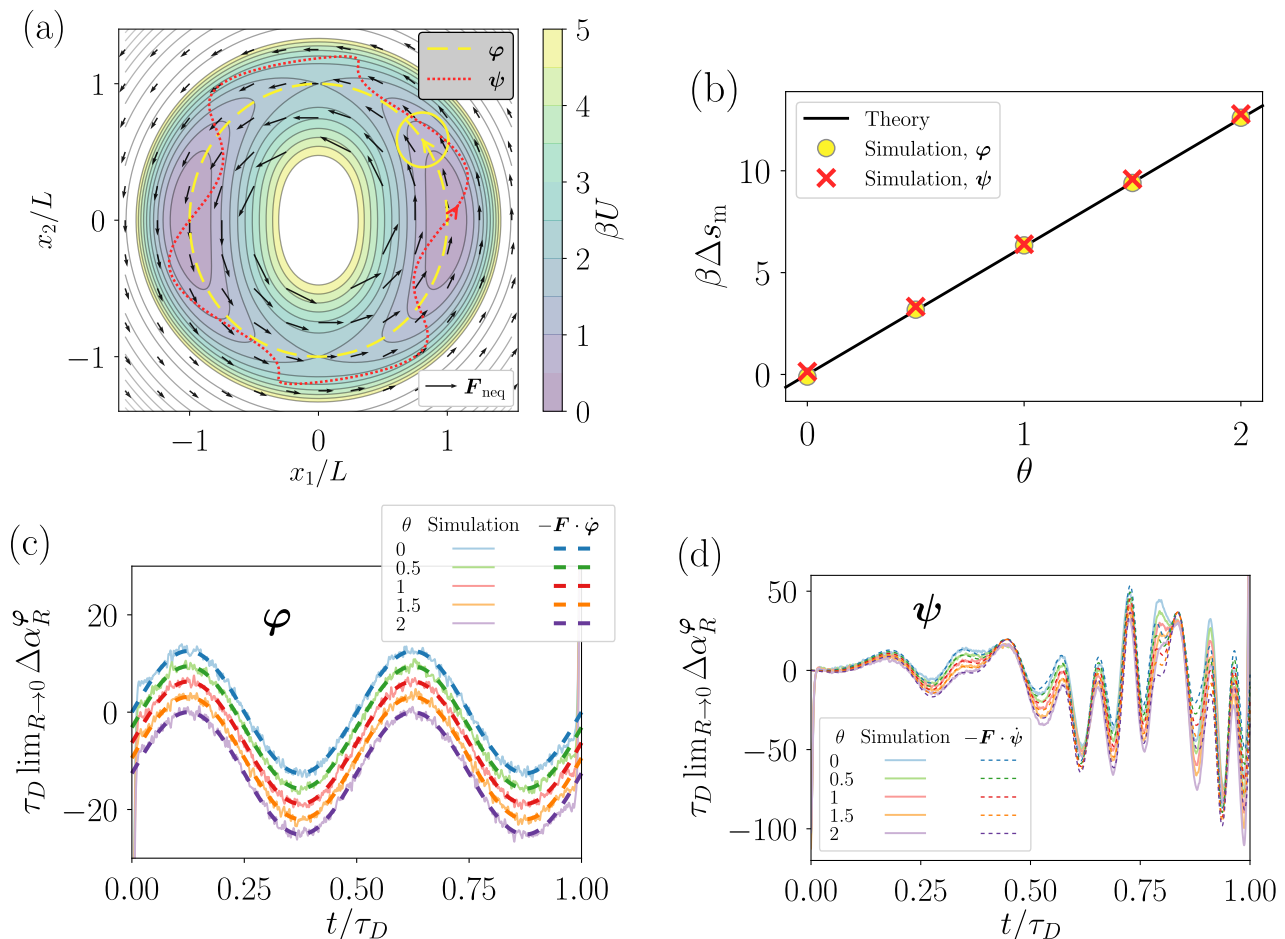


Figure 3. (a) The coloured contours show the potential  $U$  defined in Eq. (B2). The non-equilibrium force Eq. (B3) is shown as black quiver plot. The yellow dashed line denotes the path  $\varphi$  defined in Eq. (B5), the yellow circle indicates an instantaneous ball of radius  $R/L = 0.2$  around  $\varphi$ . The red dotted line denotes the path  $\psi$  defined in Eq. (B6). For both paths  $\varphi$ ,  $\psi$ , arrows indicate the forward direction. (b) The black line denotes the theoretical entropy production Eq. (B4) for  $\Gamma = 1$ . The coloured symbols denote the entropy production obtained by evaluating the right-hand side of Eq. (3) using the extrapolated measured exit rates shown in subplots (c), (d). The dots correspond to  $\varphi$ , the crosses are obtained using  $\psi$ . (c), (d) The coloured solid lines denote the extrapolation to  $R \rightarrow 0$  of measured finite-radius exit-rate differences between forward- and backward paths, for several values of  $\theta$  and the reference path (c)  $\varphi$  and (d)  $\psi$ . The coloured dashed line denotes the corresponding theoretical prediction given by the right-hand side of Eq. (8), calculated using the force Eq. (B1). Numerical data is smoothed using a Hann window of width  $0.005 \tau_D$ .

- [5] Christian Maes and Karel Netočný, “Time-Reversal and Entropy,” *Journal of Statistical Physics* **110**, 269–310 (2003).
- [6] Udo Seifert, “Entropy Production along a Stochastic Trajectory and an Integral Fluctuation Theorem,” *Physical Review Letters* **95** (2005), 10.1103/PhysRevLett.95.040602.
- [7] G N Bochkov and E Kuzovlev, “General theory of thermal fluctuations in nonlinear systems,” *Sov. Phys. JETP* **45**, 125 (1977).
- [8] C. Jarzynski, “Nonequilibrium Equality for Free Energy Differences,” *Physical Review Letters* **78**, 2690–2693 (1997).
- [9] Jorge Kurchan, “Fluctuation theorem for stochastic dynamics,” *Journal of Physics A: Mathematical and General* **31**, 3719–3729 (1998).
- [10] Gavin E. Crooks, “Entropy production fluctuation theorem and the nonequilibrium work relation for free energy differences,” *Physical Review E* **60**, 2721–2726 (1999).
- [11] Christian Maes, “On the Origin and the Use of Fluctuation Relations for the Entropy,” in *Poincaré Seminar 2003*, edited by Jean Dalibard, Bertrand Duplantier, and Vincent Rivasseau (Birkhäuser Basel, Basel, 2004) pp. 145–191.
- [12] Vladimir Y Chernyak, Michael Chertkov, and Christopher Jarzynski, “Path-integral analysis of fluctuation theorems for general Langevin processes,” *Journal of Statistical Mechanics: Theory and Experiment* **2006**, P08001–P08001 (2006).
- [13] Udo Seifert, “Stochastic thermodynamics, fluctuation theorems, and molecular machines,” *Reports on Progress in Physics* **75**, 126001 (2012), arXiv: 1205.4176.

- [14] K. Sekimoto, *Stochastic energetics*, Lecture notes in physics No. 799 (Springer, Heidelberg ; New York, 2010) oCLC: ocn462919832.
- [15] Udo Seifert, “From Stochastic Thermodynamics to Thermodynamic Inference,” *Annual Review of Condensed Matter Physics* **10**, 171–192 (2019).
- [16] D. G. Luchinsky and P. V. E. McClintock, “Irreversibility of classical fluctuations studied in analogue electrical circuits,” *Nature* **389**, 463–466 (1997).
- [17] D G Luchinsky, P V E McClintock, and M I Dykman, “Analogue studies of nonlinear systems,” *Reports on Progress in Physics* **61**, 889–997 (1998).
- [18] Shun Otsubo, Sosuke Ito, Andreas Dechant, and Takahiro Sagawa, “Estimating entropy production by machine learning of short-time fluctuating currents,” *Physical Review E* **101** (2020), 10.1103/PhysRevE.101.062106.
- [19] Sreekanth K. Manikandan, Deepak Gupta, and Supriya Krishnamurthy, “Inferring Entropy Production from Short Experiments,” *Physical Review Letters* **124** (2020), 10.1103/PhysRevLett.124.120603.
- [20] C. Tietz, S. Schuler, T. Speck, U. Seifert, and J. Wrachtrup, “Measurement of Stochastic Entropy Production,” *Physical Review Letters* **97** (2006), 10.1103/PhysRevLett.97.050602.
- [21] Julian Kappler and Ronojoy Adhikari, “Stochastic action for tubes: Connecting path probabilities to measurement,” *Physical Review Research* **2** (2020), 10.1103/PhysRevResearch.2.023407.
- [22] Jannes Gladrow, Ulrich F. Keyser, R. Adhikari, and Julian Kappler, “Direct experimental measurement of relative path probabilities and stochastic actions,” arXiv:2006.16820 [cond-mat, physics:physics] (2020), arXiv: 2006.16820.
- [23] R. Landauer, “Stability and entropy production in electrical circuits,” *Journal of Statistical Physics* **13**, 1–16 (1975).
- [24] N. G. van Kampen, “Itô versus Stratonovich,” *Journal of Statistical Physics* **24**, 175–187 (1981).
- [25] N. G. van Kampen, *Stochastic processes in physics and chemistry*, 3rd ed., North-Holland personal library (Elsevier, Amsterdam ; Boston, 2007) oCLC: ocm81453662.
- [26] Crispin W. Gardiner, *Stochastic methods: a handbook for the natural and social sciences*, 4th ed., Springer series in synergetics (Springer, Berlin, 2009).
- [27] Michael E. Cates, “Active Field Theories,” arXiv:1904.01330 [cond-mat] (2019), arXiv: 1904.01330.